J Nanopart Res (2012) 14:1253
DOI 10.1007/s11051-012-1253-2

RESEARCH PAPER

Electron transport mechanisms in individual cobalt-doped ZnO nanorods

T. Y. Ko · M.-H. Tsai · C.-S. Lee · K. W. Sun

Received: 7 May 2012 / Accepted: 15 October 2012 / Published online: 1 November 2012

Abstract This study examined carrier transport in single cobalt-doped zinc oxide (Co:ZnO) nanorods in temperatures ranging from 80 to 405 K. Measurements were taken on single nanorods deposited on a Si template, where two- and four-point metallic contacts were previously made using e-beam lithography, dielectrophoresis, and focused ion beam. In both two- and four-point probe measurements, the current–voltage curves were clearly linear and symmetrical with respect to both axes. The electrical measurements were carried out according to three different measuring methods to accurately determine the resistivity of the single Co:ZnO nanorods. The Co-doped nanorods exhibited ferromagnetic behavior at room temperature. The remanence permanent magnet of the nanorods increased with increasing Co concentration, however, this was accompanied by the decrease in electrical resistivity. The transport properties were dominated by the thermal activation of electrons from the Fermi level to the conduction band for a temperature above 140–160 K, and to the impurity band at a lower temperature. The electronic transport of the nanorods was influenced by the surface states when exposed in the air.

T. Y. Ko · M.-H. Tsai · C.-S. Lee · K. W. Sun (✉)
Department of Applied Chemistry, National Chiao Tung University, Hsinchu 30010, Taiwan
e-mail: kwsun@mail.nctu.edu.tw

Keywords Dielectrophoresis · Transport · Ferromagnetic · Co:ZnO nanorod

Introduction

Recently, there has been great interest on new types of nanodevices based on metal-oxide nanowires or nanotubes. Metal oxides with one-dimensional (1D) structures, such as nanowires, nanotubes, nanorods, and nanoribbons, demonstrate unique physical and chemical properties because of their large surface area and unique shape, making these materials effective for applications in photovoltaic devices (Leschkies et al. 2007; Law et al. 2005; Cheng et al. 2006), field emission display (Banerjee et al. 2004; Chen et al. 2008), etc. Therefore, synthesizing novel metal-oxide nanostructures and probing their intrinsic properties are critical in assessing the possible role in new types of nanoscale devices. Among these metal-oxide semiconductors, zinc oxide (ZnO) has attracted considerable interest over the years owing to its wide range of applications. This semiconductor has several favorable properties, including good transparency, high electron mobility, wide bandgap, and strong room-temperature luminescence. Those properties are used in emerging applications for transparent electrodes in liquid crystal displays, in energy-saving or heat-protecting windows, and in electronics as thin-film transistors and light-emitting diodes.

ZnO is also one of the very promising diluted magnetic semiconductors (DMSs) for spintronics applications, with many groups reporting room temperature ferromagnetism (Dietl et al. 2000; Sato and Katayama-Yoshida 2000, 2001; Sharma et al. 2003; Pearton et al. 2006). Anisotropic ferromagnetism dependent on nanowire geometry and density at room temperature was reported in Co- and Ni-doped ZnO nanowires (Cui and Gibson 2005). The magnetic properties of ZnO are still open to debate. Several models have been proposed to explain the magnetism in the DMS. It was suggested that the holes in the extended or weakly localized states mediate the long-range interaction between the localized spins on both sides of the metal–insulator-transition in the III–V magnetic semiconductor (Dietl et al. 2000). The high-temperature ferromagnetism in DMS has been analyzed in terms of the bound magnetic polaron model of indirect exchange via shallow donors, treated in a two-sublattice mean-field approximation (Coey et al. 2005). The electronic properties and magnetism of ZnO thin films and nanowires with both Zn and O vacancies were examined using first-principle theory. The origin of magnetism is attributed to the unpaired 2p electron atoms in the immediate vicinity of the Zn vacancies (Wang et al. 2008). Although single nanowires have been used as active channels in field effect transistors (Heo et al. 2004a, b; Cha et al. 2006) or logic devices (Park et al. 2005), their electrical characteristics have not yet been completely understood.

Recently, it was found that ZnO nanowires are sensitive to the measurement ambient and may be useful in gas sensing applications (Heo et al. 2004a, b; Li et al. 2004). The surface states were shown to have a pronounced effect on the electronic transport in single ZnO nanowires (Liao et al. 2007). The resistance and microstructural characterization of single ZnO nanowire prepared by thermal evaporation without use of the catalyst were investigated using nanomanipulator and transmission electron microscopy. The specific resistance was decreased with increasing rapid thermal annealing (RTA) temperature and dropped abruptly at the RTA temperature above 500 °C (Yoon et al. 2009). The DC electrical conductivity of a nanowire synthesized by chemical vapor deposition was investigated from 300 to 6 K. It was found that the electron conduction in the wire was dominated by the Efros–Shklovskii variable-range hopping mechanism with a large apparent Coulomb gap (Ma et al. 2005). The temperature behavior of resistivity in both the semiconducting and the metallic-like single-crystalline individual ZnO nanowires were studied using the four-probe method (Chiu et al. 2009). The transport measurements revealed that the electrical transport mechanisms through individual ZnO nanowires were due to a combination of the thermal activation conduction and the nearest-neighbor hopping (NNH) conduction processes. Above 100 K, the charge transport was dominated by the thermal activation of electrons from the Fermi level to the conduction band.

Many groups have studied the electrical properties of ZnO-based nanostructures; however, the results differ significantly (Schlenker et al. 2008). Moreover, there are only a very small number of experimental results reported on ZnO DMS nanostructures. It is only very recently that electrical and magnetotransport measurements were performed on single Co-doped ZnO DMS nanowires (Liang et al. 2009). The activation energy retrieved from the temperature-dependent resistance measurements between 5 and 300 K varied from 38 to 45 meV.

In this present work, resistivity and contact resistance of single Co:ZnO nanorods with different Co doping concentrations were accurately determined using three different probe schemes over a wide temperature range from 405 to 80 K. Electron transport mechanisms in ZnO DMS nanorods were fully analyzed through DC electrical conductivity and temperature-dependent current–voltage (*I–V*) curve measurements.

Experimental

The Co:ZnO nanorod samples studied in this work were prepared by the hydrothermal method. Zinc nitrate hydrate ($Zn(NO_3)_2$, 0.06 g) and HMTA (hexamethylenetetramine, 0.028 g) were added to 40 mL of deionized (DI) water to form a 5 mM clear solution. In the experiment, ZnO nanorods of three different doping concentrations were made using cobalt nitrate with weight percentages of 10 (sample A), 60 (sample B), and 90 (sample C) with respect to zinc nitrate hydrate dissolved into the above solution. The mixture was heated in a Teflon-coated stainless steel autoclave at 95 °C for 2 h. After cooling to room temperature, the solid product was put into a centrifuge tube and was repeatedly cleaned with DI water to wash away

the remaining Co ions between 5 and 10 times, depending on the amount of cobalt nitrate added. The solid was dried at 70 °C for 5 h to obtain the Co-doped ZnO nanorod powder. Doping concentration varied by adjusting the weight percentage of the cobalt nitrate. The color of the ZnO nanorod powder turned green as the doping became heavier. The composition of the solid was found by powder X-ray diffraction (XRD) to be ZnO. The doping concentration of Co was analyzed using inductively coupled plasma mass spectroscopy. The mole fractions of Co in samples A, B, and C were 0.02 %, 0.1 %, and 0.2 %, respectively.

The strong peaks in the XRD patterns (as shown in Fig. 1a) indicate that well-aligned ZnO nanorods with wurtzite structures were obtained and that the crystal structures were not altered by the doping. The chemical compositions of the nanorods are also supported from the results of energy dispersive spectroscopy (as shown in Fig. 1b). The scanning electron microscope (SEM) image of the fabricated nanorods is shown in Fig. 2. The nanorods were uniform in size, with a diameter of approximately 200 nm. However, the length of the rod varied from 6 to 1 μm as the doping weight percentage was increased from 0 to 90. The oxidation state of the Co ions was varied to be 2+ using the X-ray absorption spectroscopy (data not shown here). The Co ions indeed substitute the Zn ion sites in the nanorods. Results from measurements using a superconducting quantum interference device indicate the hysteresis behavior of Co-doped ZnO nanorods with different doping levels at room temperature, as shown in Fig. 3. The sample exhibited weak ferromagnetic behavior with remanent magnetization in the order of 10^{-3} emu/g.

Fabrication processes of the single nanorod-based devices for the electrical measurements are given as follows. The nanorod powder was first diluted in 10 mL DI water and ethanol mixture. The solution was then placed in an ultrasonic bath operated at a vibration frequency of 185 kHz for 15 min to prevent cluster formation. A test drop of the solution was placed on a bare Si wafer. After the solution dried out, SEM images were taken to examine nanowire clustering. The concentration of the solution was continuously diluted and adjusted until the nanostructures could be well dispersed on the Si template.

Two- and four-point metal contacts on Si templates were designed and fabricated to position dispersed single nanorods. The templates used were commercially available 4-in. silicon wafers with (001) crystal orientation and n-type background doping. The surface of the Si substrate was passivated in advance using a thermally grown SiO_2 layer with a thickness of 1,200 Å. This was to avoid leakage of I through the substrate during I–V measurements. The Si wafer was first diced into 2×2 cm chips. A pattern of 2D arrays of cross-finger-type Ti/Au pads which served as the two- and four-point contact devices with a line width of ~ 1 μm, a pitch from 0.8 to 1.5 μm, and a length of ~ 15 μm were defined on the Si chip using e-beam lithography and lift-off technique within an area of 1 mm^2.

A drop of 3 μL properly diluted ZnO nanorod solution was placed within the inter-digitated electrode patterns. By applying an AC electrical bias (10 MHz, 6 V peak to peak) across the contact pads, the dielectrophoresis force (Yamamoto et al. 1996, 1998; Choi et al. 2001; Suehiro et al. 2003) drove the nanorods to bridge the electrode gap. The sample surface was scanned by SEM to allocate single nanorods across two or four metal contacts. After single nanorods were selected, a focus ion beam (FIB) was used to selectively deposit platinum (Pt) metal contacts on the rods. The patterned single nanorods were examined with EDX to ensure they were not contaminated during the FIB process. Temperature dependence of the I–V characteristics of individual ZnO nanorods was probed at a temperature range from 80 to 405 K. This was done with a KEITHLEY 6430 probe station under I sensitivity of 1 pA and a Linkam THMS600 heating and freezing stage with a Linkam TP94 temperature programmer. The resistivity of single nanorods was determined with three different probe schemes: (a) two-point contact probe (sweep V mode), where I through the wire was measured by sweeping the V from -1.0 to $+1.0$ V with a step of 0.01 V; (b) four-point contact probe (sweep I mode), where I was supplied through outer electrodes and V drop was determined between two inner electrodes; and (c) four-point contact probe, where resistivity of the nanowire was determined using a developed algorithm (Gu et al. 2006).

Results and discussion

Figure 4 shows the schematic, SEM image, and I–V response of a single undoped ZnO nanorod prepared on two-point contact Au/Ti electrodes. At room temperature, contacts between the nanorods and

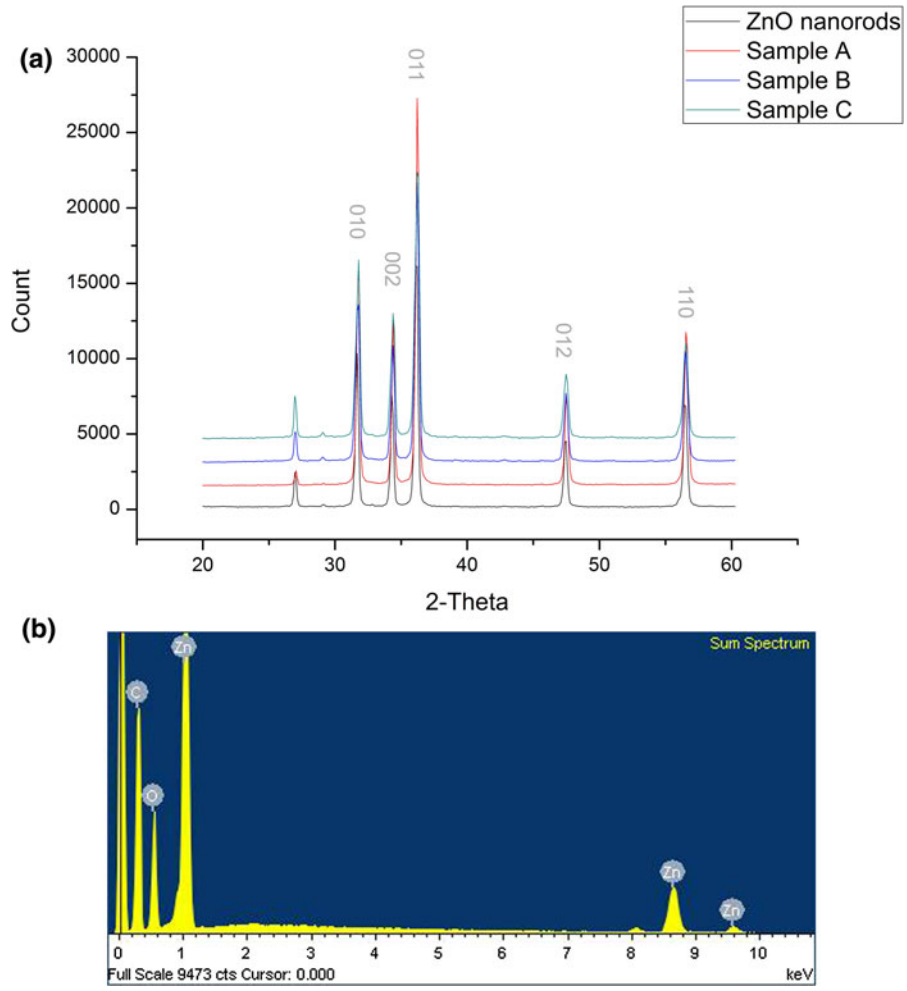

Fig. 1 XRD patterns and EDX spectrum of the fabricated Co:ZnO nanorods

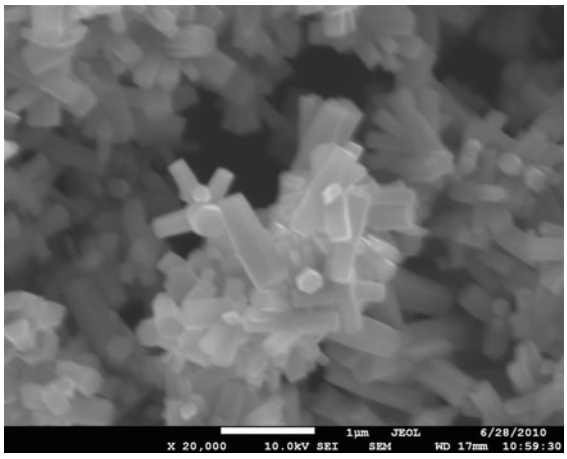

Fig. 2 SEM *image* of the fabricated Co:ZnO nanorods

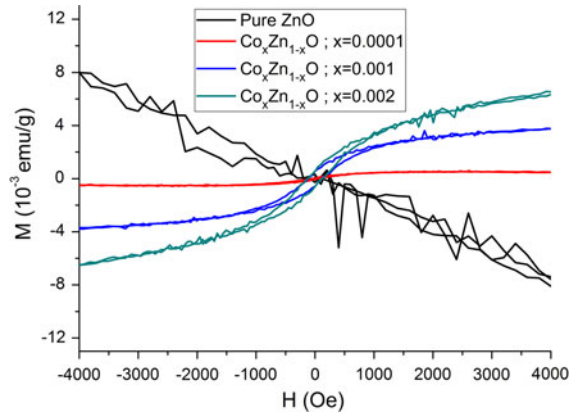

Fig. 3 Hysteresis behavior of Co:ZnO nanorods at room temperature. The undoped sample is also displayed in parallel for comparison

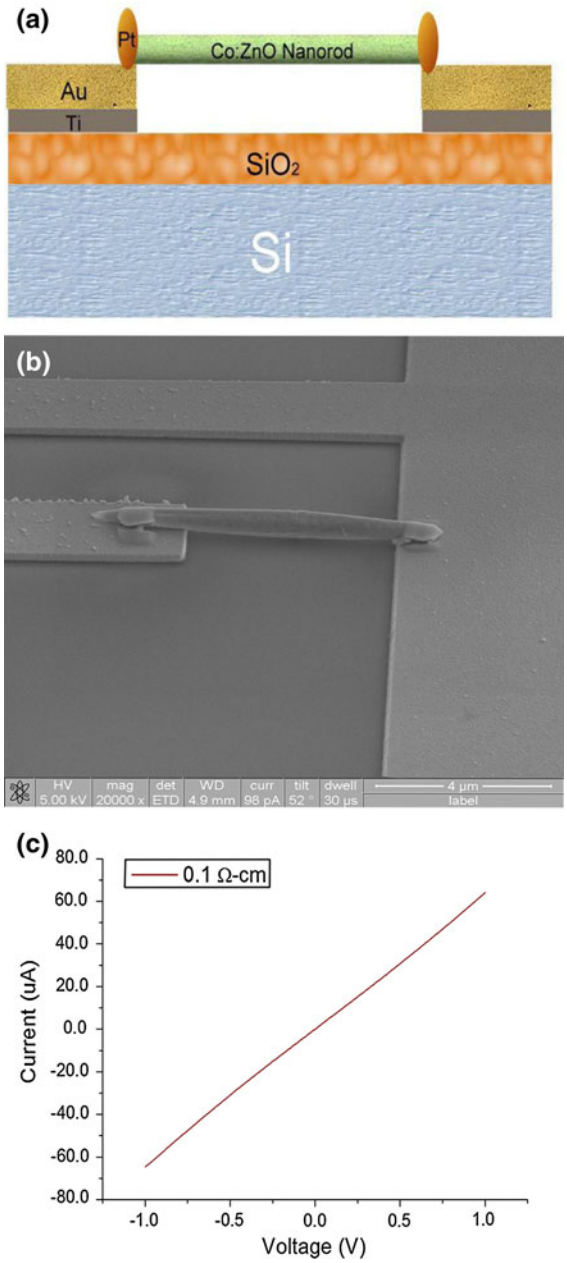

Fig. 4 **a** Schematic, **b** SEM *image* and **c** *I–V* response of a single undoped ZnO nanorod prepared on two-point contact probe Au/Ti electrodes

the electrodes show linear and symmetrical behavior. A distribution of resistivity from 0.1 to 0.636 Ω cm was derived from various single undoped ZnO nanorods. Measurements implemented with the same probing scheme were also carried out on Co-doped samples. The relevant measured values for the doped nanorods are listed in Table 1. The parameters from the undoped ZnO nanorods are displayed together for comparison. A small spreading in the values of resistivity among samples with the same doping parameter is attributed to the slight difference in the numbers of oxygen vacancies and Zn interstitials, which affect the carrier concentrations in the nanorods. Nevertheless, they all fall within the same order of magnitude. From Table 1, it is noted that the resistivity rises with the increasing Co concentrations. Similar behavior was also observed in Co-doped ferromagnetic ZnO films, in which the resistivity of the films was found to increase with Co doping (MacManus-Driscoll et al. 2007). Co^{2+} typically forms deep levels in the bandgap of ZnO. We speculate that the increase in resistivity of the ZnO nanorods is due to localization of carriers with increasing Co doping. Note that the increasing Co doping also leads to stronger magnetic moments, saturation magnetization, and coercive force (as listed in Table 1). Although connections between ferromagnetic transition and transport properties in the DMS system with localized carriers have been theoretically studied (Kaminski and Das Sarma 2003). However, more experimental evidences are needed to resolve this issue.

Note that measured resistances from the two-point probe scheme contain contributions from the resistances of the nanorods as well as from the contact resistances. Contact resistances can be determined by comparing results between two- and four-point probe measurements. For example, the values of resistivity from an undoped single rod determined with probe schemes (a) and (b) are 0.636 and 0.618 Ω cm, respectively, resulting in a negligible contact resistance. The resistivity value was further verified using probe scheme (c). The schematic of probe scheme (c) and the parameters used to derive the resistivity on the same undoped nanorod are summarized in Fig. 5. The derived resistivity is 0.638 Ω cm, which is also very close to the result determined from probe schemes (a) and (b). Therefore, we conclude that the resistivity of single nanorods in these experiments can be accurately determined by simply using the probe scheme (a).

Following the electrical characterization of the single rods at room temperature, individual nanorods were placed on a cooling/heating stage in a chamber. Measurements of temperature dependence in conductivity were first carried out in a vacuum in temperatures ranging from 300 to 80 K. Figure 6 displays the *I–V*

Table 1 List of measured parameters of the un- and Co-doped ZnO nanorods from the experiments

Sample numbers	Co-doped concentrations (%)	Distribution of resistivity (Ω cm)	Saturation magnetization (in powder form) (emu/g)	Coercive force (in powder form) (Oe)
Pure	0	0.636–0.1	0	0
Sample A	0.02	0.6–0.126	5.0×10^{-4}	50
Sample B	0.1	25–63	2.0×10^{-3}	125
Sample C	0.2	15.52–150	2.9×10^{-3}	125

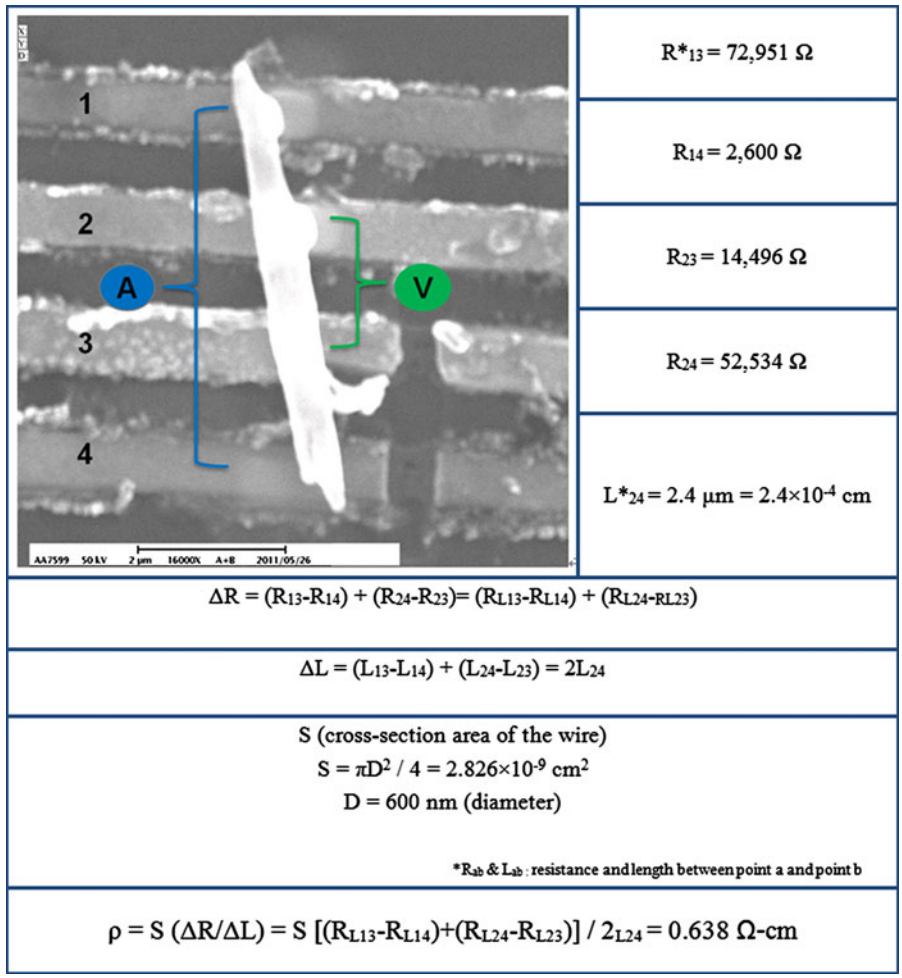

Fig. 5 Schematic of probe scheme **c** and the parameters used to derive the resistivity on the undoped ZnO nanorod

curves of samples A, B, and C on two-point probe electrodes. The resistance of the single nanorods is also plotted in Figs. 7, 8, and 9 as ln(R) versus reciprocal temperature for all three samples. A decrease in conductivity with decreasing temperature was revealed, which seems to be consistent with the thermally activated transport model. However, the curve departed significantly from linearity when the curves in Figs. 7, 8, and 9 were analyzed (as shown in the inset of Figs. 7, 8, and 9) using a simplified equation (Chiu et al. 2009) for natively doped ZnO nanowires by ignoring the third term and setting $\eta_3 = \infty$: $\eta^{-1}(T) = \eta_1^{-1} e^{\frac{-E_1}{K_B T}} + \eta_2^{-1} e^{\frac{-E_2}{K_B T}} + \eta_3^{-1} e^{\frac{-E_3}{K_B T}}$, where η_i ($i = 1, 2, 3$) are temperature-independent resistivity parameters, and E_i are thermal activation energies

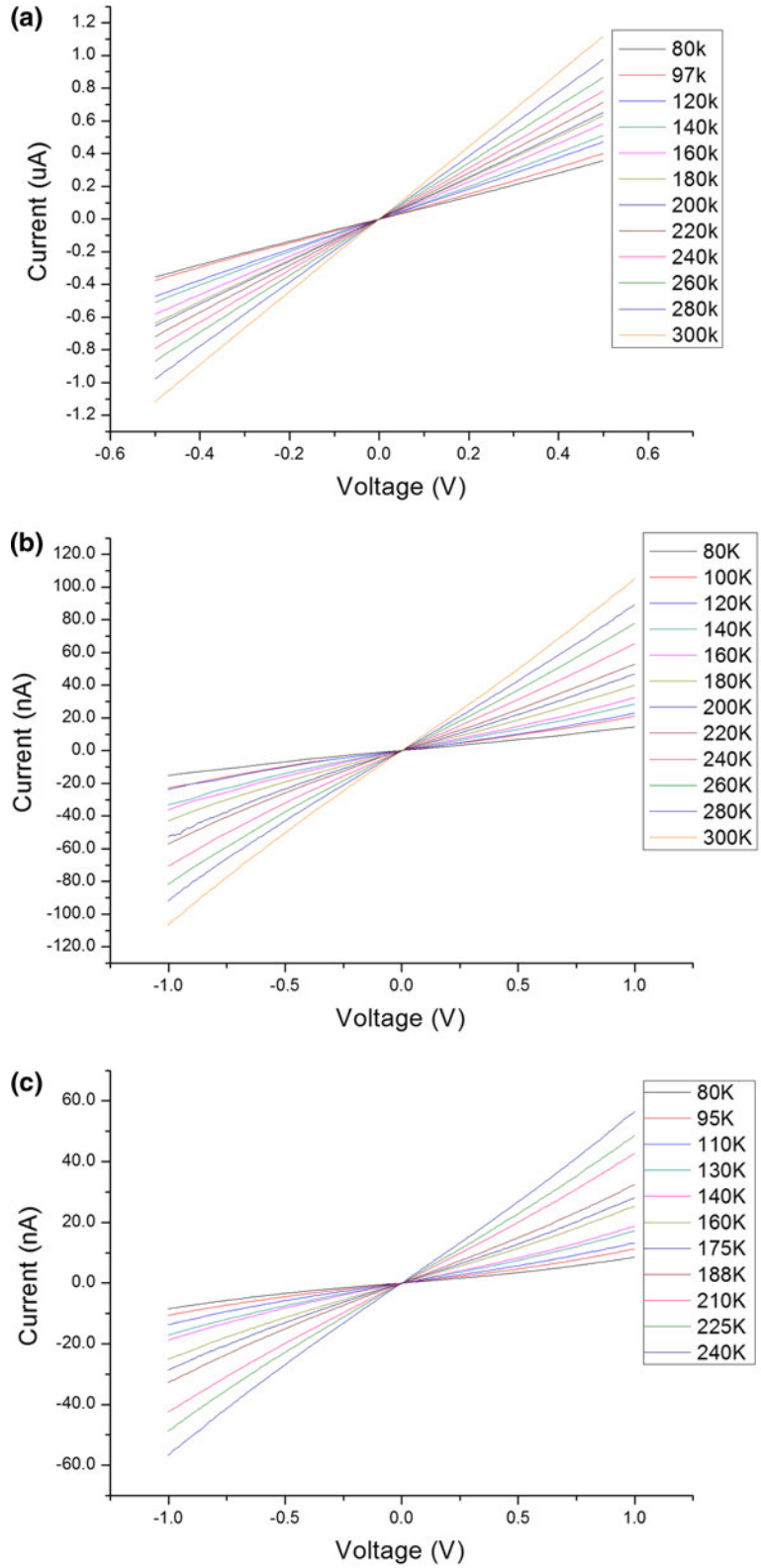

Fig. 6 **a–c** Temperature-dependent *I–V* characteristics of samples A, B, and C on two-point probe electrodes

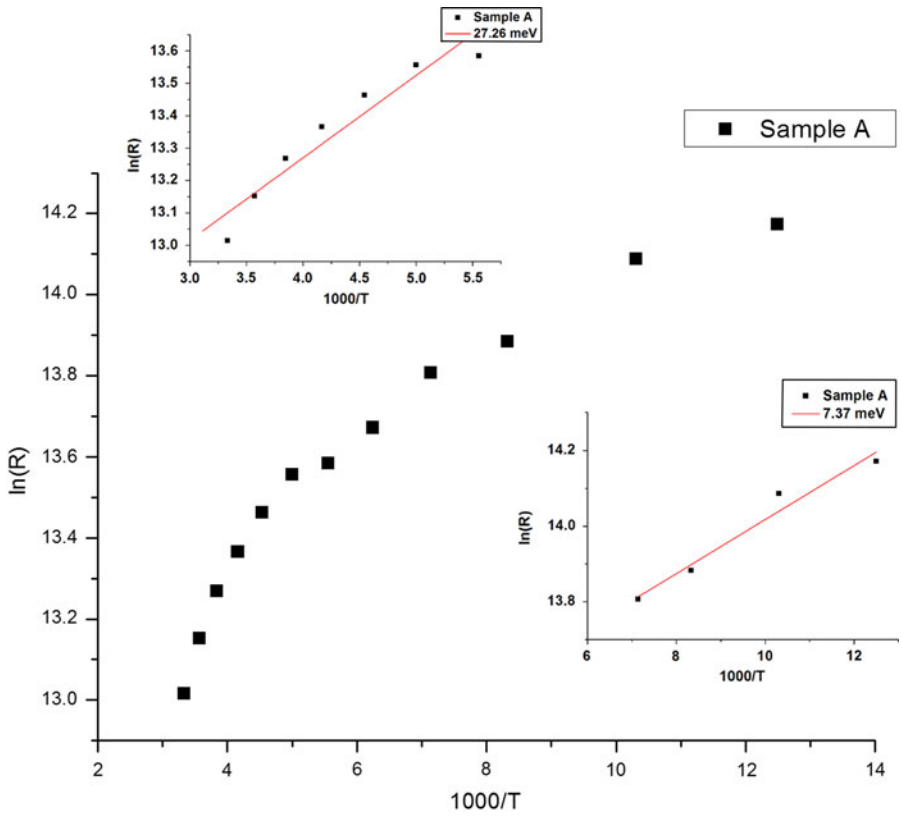

Fig. 7 Resistance variations with reciprocal temperature for sample A. The *insets* show the fitting for activation energies in the temperature range of 300–160 and 160–80 K

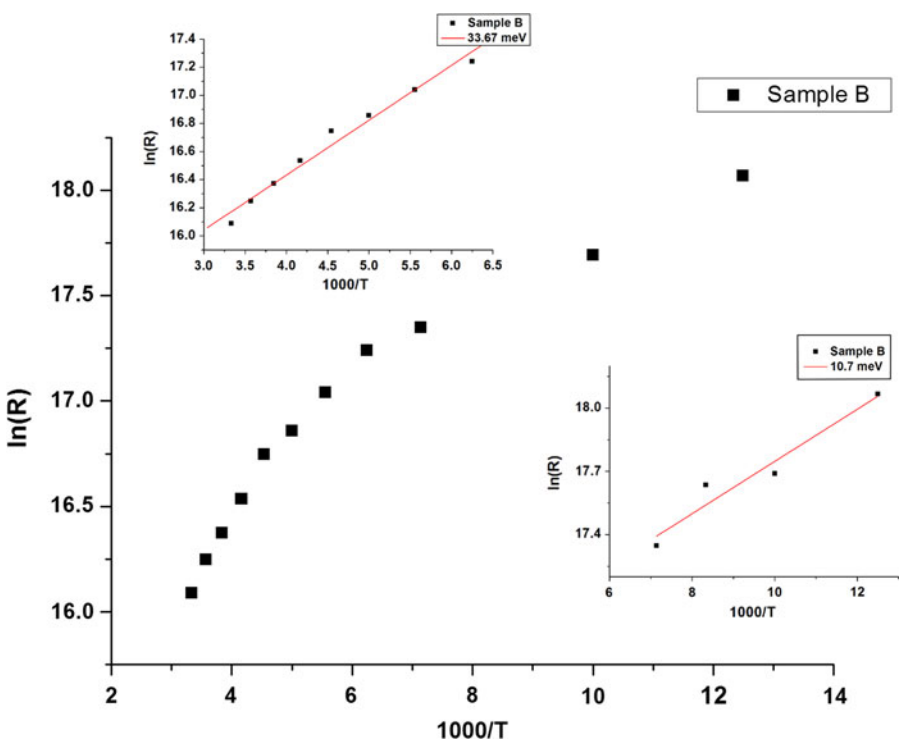

Fig. 8 Resistance variations with reciprocal temperature for sample B. The *insets* show the fitting for activation energies in the temperature range of 300–140 and 140–80 K

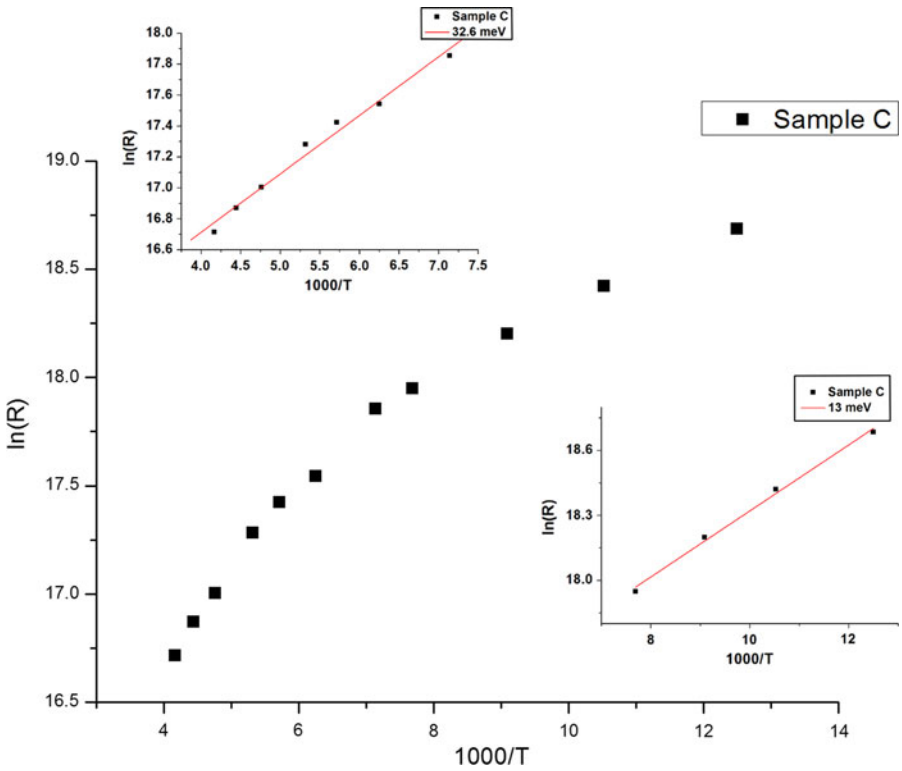

Fig. 9 Resistance variations with reciprocal temperature for sample C. The *insets* show the fitting for activation energies in the temperature range of 300–140 and 140–80 K

Table 2 List of experimental values of activation energies (E_i) and temperatures of *curve* turning points for samples A, B, and C

Sample numbers	E_1 (meV)	E_2 (meV)	Temperature turning point (K)
Sample A	27.26	7.37	160
Sample B	33.67	10.7	140
Sample C	32.6	13	140

describing the electronic conduction in intermediate (E_1) and low (E_2) temperature regimes. Note that $E_1 > E_2 > E_3$ and $\eta_1 \ll \eta_2 \ll \eta_3$, as is evident in Figs. 7, 8, and 9. Experimental values of the activation energies (E_i) and temperatures where the change of linearity took place for samples A, B, and C are listed in Table 2. Note that the activation energies were not significantly affected by the Co doping levels.

The electrical transport processes can be explained as follows. In the intermediate temperature regime (300–140 K), the electrons are thermally excited from the Fermi level (the donor ground state) to the conduction band where abundant unoccupied, extended states with high mobilities are available. This thermal activation process dominates the measured E_1 transport channel. The measured values of activation energy E_1s are in good agreement with recent published results (Chiu et al. 2009; Chang and Lu 2008; Liang et al. 2009) based on the *I* knowledge of the ionization for the shallow donors in the ZnO materials. As the temperature drops below 140 or 160 K, carriers are no longer allowed to be excited to the conduction band by the thermal energy K_BT. However, the electron can be excited from the Fermi level to the shallow donor impurity band (Nishimura 1965; Shklovskii and Efros 1984; Hung and Gliessman 1954; Mott and Davis 1979) where unoccupied states are available. As a result, the E_2 transport process begins to dominate the low temperature regime (160–80 K). Due to instrument limitations, we were not able to observe different transport processes where the NNH process was expected to be the dominant one at temperature below 20 K (Chiu et al. 2009).

In the next experiments, the sample chamber was pumped down and flushed with dry N_2 three times. The temperature-dependent measurements in conductivity of sample A were carried out both in vacuum and at an inert gas (N_2) filled environment at high temperatures ranging from 300 to 405 K. Figure 10 shows the *I–V* curve and resistance of the single nanorod

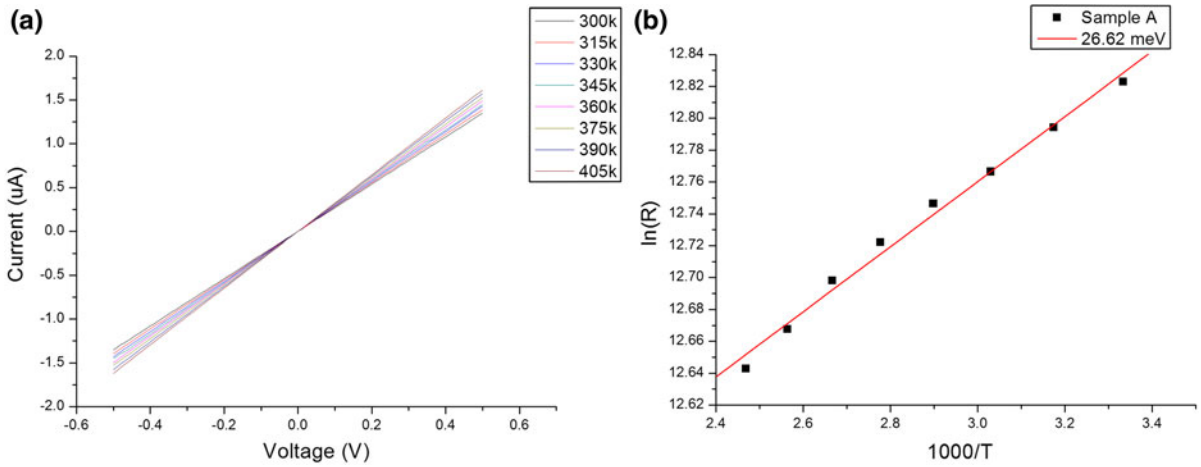

Fig. 10 **a** *I–V curve* and **b** resistance variation with reciprocal temperature for the undoped ZnO nanorod between 300 and 405 K

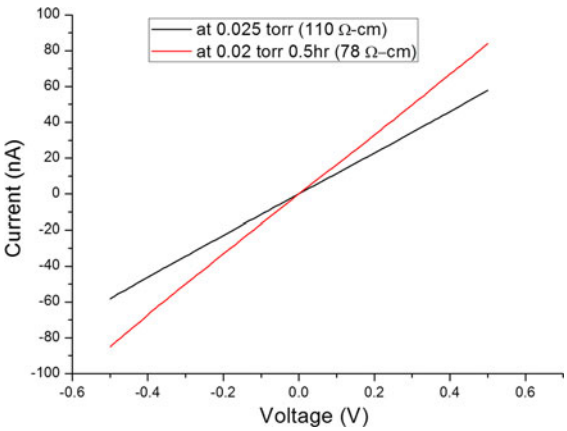

Fig. 11 *I–V* response of sample C in vacuum

plotted as ln(R) versus reciprocal temperature. The resistance of the nanorod dropped from 0.37 MΩ at 300 K to 0.31 MΩ at 405 K. The activation energy retrieved from the curve in Fig. 10 is approximately 26.62 meV, which is close to the values obtained in the intermediate temperature regime. Therefore, it is concluded that for temperatures above 300 K, the conduction channel is also dominated by the thermal activation transport process.

On the other hand, it was also found that the resistance of all the samples slowly increased when they were exposed in the air for a period of time. For example, when sample C was left in the air for 3 weeks, its resistivity increased from 15.52 to 116 Ω cm. The resistivity further increased to 126 Ω cm on the 22nd day. It was speculated that this was likely due to the adsorption of oxygen on the nanorod surface (Yuan et al. 2008; Bao et al. 2011; Kind et al. 2002). In order to verify the effect of surface adsorption, resistivity of sample C, after been exposed in the air for 22 days, was measured again by placing it in vacuum. The measured resistivity immediately dropped from 126 to 110 Ω cm when the vacuum level reached a pressure of 25 mT, as shown in Fig. 11. With the sample kept at a vacuum level of 20 mT for another half an hour, the resistivity further decreased to 78 Ω cm. However, the resistivity was never able to totally recover to its original value even when left under a vacuum over several months. This experiment indicates that surface adsorptions have a significant effect on the transport properties of Co:ZnO nanorods.

Summary

In conclusion, the transport properties and temperature dependence in conductivity of single Co:ZnO nanorods using e-beam lithography, FIB, and dielectrophoresis techniques were reported. *I–V* characteristics showed linear and symmetric behavior through the entire temperature range. The resistivity and contact resistance were accurately determined using three different probe schemes. As the temperature was gradually reduced from 405 to 80 K, the charge transport processes changed from the conduction- to the impurity-band channel. Considering the significant contribution of surface adsorption to conductivity, methods of surface modification may be used to

effectively manipulate the electrical properties of Co:ZnO nanorods.

Acknowledgments This work was supported by a Grant from the National Science Council of the Republic of China under Grant No. NSC 99-2119-M-009-004-MY3 and the MOE ATU Program.

References

Banerjee D, Jo SH, Ren ZF (2004) Enhanced field emission of ZnO nanowires. Adv Mater 16:2028–2032

Bao J, Shalish I, Su Z, Gurwitz R, Capasso F, Wang X, Ren Z (2011) Photoinduced oxygen release and persistent photoconductivity in ZnO nanowires. Nanoscale Res Lett 6:404

Cha SN, Jang JE, Choi Y, Amaratunga GAJ, Ho GW, Welland ME, Hasko DG, Kang D-J, Kim JM (2006) High performance ZnO nanowire field effect transistor using self-aligned nanogap gate electrodes. Appl Phys Lett 89:263102

Chang P-C, Lu JG (2008) Temperature dependent conduction and UV induced metal-to-insulator transition in ZnO nanowires. Appl Phys Lett 92:212113

Chen W, Zhou CW, Mai LQ, Liu YL, Qi YY, Dai Y (2008) Field emission from $V_2O_5{\cdot}nH_2O$ nanorod arrays. J Phys Chem C 112:2262–2265

Cheng K, Chen F, Kai J (2006) V_2O_5 nanowires as a functional material for electrochromic device. Sol Energy Mater Sol Cells 90:1156–1165

Chiu S-P, Lin Y-H, Lin J-J (2009) Electrical conduction mechanisms in natively doped ZnO nanowires. Nanotechnology 20:015203

Choi WB, Jin YW, Kim HY, Lee SJ, Yun MJ, Kang JH, Choi YS, Park NS, Lee NS, Kim JM (2001) Electrophoresis deposition of carbon nanotubes for triode-type field emission display. Appl Phys Lett 78:1547

Coey JMD, Venkatesan M, Fitzgerald CB (2005) Donor impurity band exchange in dilute ferromagnetic oxides. Nat Mater 4:173–179

Cui JB, Gibson UJ (2005) Electrodeposition and room temperature ferromagnetic anisotropy of Co and Ni-doped ZnO nanowire arrays. Appl Phys Lett 87:133108

Dietl T, Ohno H, Matsukura F, Cibert J, Ferrand D (2000) Zener model description of ferromagnetism in Zinc-Blende magnetic semiconductors. Science 287:1019–1022

Gu W, Choi H, Kim K (2006) Universal approach to accurate resistivity measurement for a single nanowire: theory and application. Appl Phys Lett 89:253102

Heo YW, Tein LC, Kwon Y, Norton DP, Pearton SJ, Kang BS, Ren F (2004a) Depletion-mode ZnO nanowire field-effect transistor. Appl Phys Lett 85:2274–2276

Heo YW, Tien LC, Norton DP, Kang BS, Ren F, Gila BP, Pearton SJ (2004b) Electrical transport properties of single ZnO nanorods. Appl Phys Lett 85:2002–2004

Hung CS, Gliessman JR (1954) Resistivity and Hall effect of germanium at low temperatures. Phys Rev 96:1226–1236

Kaminski A, Das Sarma S (2003) Magnetic and transport percolation in diluted magnetic semiconductors. Phys Rev B 68:235201

Kind H, Yan H, Messer B, Law M, Yang P (2002) Nanowire ultraviolet photodetectors and optical switches. Adv Mater 14:158–160

Law M, Greene LE, Johnson JC, Saykally R, Yang P (2005) Nanowire dye-sensitized solar cells. Nat Mater 4:455–459

Leschkies KS, Divakar R, Basu J, Enache-Pommer E, Boercker JE, Carter CB, Kortshagen UR, Norris DJ, Aydil ES (2007) Photosensitization of ZnO nanowires with CdSe quantum dots for photovoltaic devices. Nano Lett 7:1793–1798

Li QH, Wan Q, Liang YX, Wang TH (2004) Electronic transport through individual ZnO nanowires. Appl Phys Lett 84:4556–4558

Liang W, Yuhas BD, Yang P (2009) Magnetotransport in Co-doped ZnO nanowires. Nano Lett 9:892–896

Liao Z-M, Liu K-J, Zhang J-M, Xu J, Yu D-P (2007) Effect of surface states on electron transport in individual ZnO nanowires. Phys Lett A 367:207–210

Ma Y-J, Zhang Z, Zhou F, Lu L, Jin A, Gu C (2005) Hopping conduction in single ZnO nanowires. Nanotechnology 16:746–749

MacManus-Driscoll JL, Khare N, Liu Y, Vickers ME (2007) Structural evidence for Zn interstitials in ferromagnetic $Zn_{1-x}Co_xO$ films. Adv Mater 19:2925–2929

Mott NF, Davis EA (1979) Electronic processes in non-crystalline materials. Clarendon Press, Oxford

Nishimura H (1965) Impurity conduction in the intermediate concentration region. Phys Rev 138:A815–A821

Park WI, Kim JS, Yi GC, Lee H-J (2005) ZnO nanorod logic circuits. Adv Mater 17:1393–1397

Pearton SJ, Norton DP, Heo YW, Tien LC, Ivill MP, Li Y, Kang BS, Ren F, Kelly J, Hebard AF (2006) ZnO spintronics and nanowire devices. J Electron Mater 35:862–868

Sato K, Katayama-Yoshida H (2000) Material design for transparent ferromagnets with ZnO-based magnetic semiconductors. Jpn J Appl Phys 2 2(39):L555–L558

Sato K, Katayama-Yoshida H (2001) Stabilization of ferromagnetic states by electron doping in Fe-, Co- or Ni-doped ZnO. Jpn J Appl Phys 2 40:L334–L336

Schlenker E, Bakin A, Weimann T, Hinze P, Weber DH, Gölzhäuser A, Wehmann H-H, Waag A (2008) On the difficulties in characterizing ZnO nanowires. Nanotechnology 19:365707

Sharma P, Gupta A, Rao KV, Owens FJ, Sharma R, Ahuja R, Osorio Guillen JM, Johansson B, Gehring GA (2003) Ferromagnetism above room temperature in bulk and transparent thin films of Mn-doped ZnO. Nat Mater 2:673–677

Shklovskii BI, Efros AL (1984) Electronic properties of doped semiconductors. Springer, New York

Suehiro J, Zhou GB, Hara M (2003) Fabrication of a carbon nanotube-based gas sensor using dielectrophoresis and its application for ammonia detection by impedance spectroscopy. J Phys D 36:L109–L114

Wang Q, Sun Q, Chen G, Kawazoe Y, Jena P (2008) Vacancy-induced magnetism in ZnO thin films and nanowires. Phys Rev B 77:205411

Yamamoto K, Akita S, Nakayama Y (1996) Orientation of carbon nanotubes using electrophoresis. Jpn J Appl Phys 2 35:L917–L918

Yamamoto K, Akita S, Nakayama Y (1998) Orientation and purification of carbon nanotubes using AC electrophoresis. J Phys D 31:L34–L36

Yoon SW, Seo JH, Kim K-H, Ahn J-P, Seong TY, Lee KB, Kwon H (2009) Electrical properties and microstructural characterization of single ZnO nanowire sensor manufactured by FIB. Thin Solid Films 517:4003–4006

Yuan GD, Zhang WJ, Jie JS, Fan X, Zapien JA, Leung YH, Luo LB, Wang PF, Lee CS, Lee ST (2008) p-Type ZnO nanowire arrays. Nano Lett 8:2591–2597